

III-V photonic integrated circuit with waveguide-coupled light-emitting diodes and WSi superconducting single-photon detectors F

Cite as: Appl. Phys. Lett. **115**, 081105 (2019); <https://doi.org/10.1063/1.5108893>

Submitted: 03 May 2019 . Accepted: 07 August 2019 . Published Online: 22 August 2019

Corey McDonald, Galan Moody, Sae Woo Nam, Richard P. Mirin, Jeffrey M. Shainline , Adam McCaughan , Sonia Buckley, and Kevin L. Silverman

COLLECTIONS

 This paper was selected as Featured

 This paper was selected as Scilight



View Online



Export Citation



CrossMark

ARTICLES YOU MAY BE INTERESTED IN

[High power GaInNAs superluminescent diodes emitting over 400 mW in the 1.2 \$\mu\text{m}\$ wavelength range](#)

Applied Physics Letters **115**, 081104 (2019); <https://doi.org/10.1063/1.5111012>

[InAsSb-based heterostructures for infrared light modulation](#)

Applied Physics Letters **115**, 081102 (2019); <https://doi.org/10.1063/1.5111980>

[Hybrid silicon on silicon carbide integrated photonics platform](#)

Applied Physics Letters **115**, 141105 (2019); <https://doi.org/10.1063/1.5116201>



Your Qubits. Measured.

Meet the next generation of quantum analyzers

- Readout for up to 64 qubits
- Operation at up to 8.5 GHz, mixer-calibration-free
- Signal optimization with minimal latency

Find out more



III-V photonic integrated circuit with waveguide-coupled light-emitting diodes and WSi superconducting single-photon detectors



Cite as: Appl. Phys. Lett. **115**, 081105 (2019); doi: 10.1063/1.5108893
Submitted: 3 May 2019 · Accepted: 7 August 2019 ·
Published Online: 22 August 2019



View Online



Export Citation



CrossMark

Corey McDonald,^{1,2} Galan Moody,² Sae Woo Nam,² Richard P. Mirin,² Jeffrey M. Shainline,² 
Adam McCaughan,²  Sonia Buckley,^{2,a)} and Kevin L. Silverman^{1,2,a)}

AFFILIATIONS

¹Department of Physics, University of Colorado, Boulder, Colorado 80309, USA

²National Institute of Standards and Technology, Boulder, Colorado 80305, USA

^{a)}Electronic addresses: sonia.buckley@nist.gov and kevin.silverman@nist.gov

ABSTRACT

We demonstrate cryogenic, all on-chip, single-photon-level photonic integrated circuits on a III-V platform with waveguide-coupled quantum-well sources and tungsten silicide superconducting nanowire single-photon detectors. We have measured the dark count rates below 10^{-3} counts/s and have reduced the cross talk to an adjacent waveguide by 30 dB.

<https://doi.org/10.1063/1.5108893>

A photonic integrated circuit (PIC) platform that incorporates superconducting single-photon detectors and quantum sources in an all-electrical, all on-chip package would be of great benefit for quantum optical research science and advanced computing. Improvements in microfabrication have allowed quantum optical experiments such as Hanbury-Brown and Twiss (HBT)^{1–4} and Hong-Ou-Mandel interferometry,^{5,6} as well as photonic quantum information processors to be replicated in a cubic centimeter-scale package at cryogenic temperatures.⁷ A scalable demonstration of a PIC platform for quantum optical experiments and advanced computing requires electrically injected single-photon emitters,^{8–10} single-photon detectors with low dark count rates and high quantum efficiency,^{11,12} and low-loss waveguides for routing. As an applied technology, fully integrated PICs would be useful as a modular platform for photonic quantum computing and high-performance neuromorphic computing.¹³ Furthermore, optical isolation between unintentionally coupled source-detector pairs is necessary to ensure reliable operation and precision measurements. While photonic circuits and the performance of integrated detectors have rapidly advanced, slow development of on-chip, electrically pumped light sources has hampered progress toward a fully integrated source-detector circuit.

A proof-of-principle, fully integrated, source-detector PIC has been previously demonstrated on a silicon platform using *W*-center defects as emissive centers in light-emitting diode (LED) structures.¹⁴ Silicon waveguides are weakly absorbing at the $1.2\ \mu\text{m}$ emission wavelength of the *W*-centers and can route light to single-photon detectors

without significant loss. While *W*-centers can emit light at cryogenic temperatures and may have potential as single-photon emitters, they suffer from a low electrical-to-optical efficiency,¹⁵ which reduces the total system efficiency. To circumvent these limitations, source-detector PICs using waveguide-integrated III-V quantum dots (QDs) as single-photon emitters have also been pursued,^{16–18} however, single photons were generated from the QDs via external optical pumping, which leads to substantial scattered pump light on integrated detectors that has prevented fully integrated chip-scale quantum optical experiments. Furthermore, niobium nitride single-photon detectors on III-V platforms typically lack a saturable internal quantum efficiency and suffer worse dark count rates compared to tungsten silicide (WSi) detectors.^{10,19,20} Here, we demonstrate a III-V PIC platform with waveguide-coupled LED light sources and high-efficiency superconducting-nanowire single-photon detectors (SNSPDs) that exhibit dark count rates below 10^{-3} counts/s with greater than 30 dB cross talk isolation between adjacent channels. Our devices use an all on-chip, waveguide-integrated *p-i-n* LED coupled to amorphous WSi SNSPDs^{21–23} for an electrical-optical-electrical cryogenic PIC with excellent signal-to-noise ratios from low dark counts, highly isolated waveguides, and high quantum efficiency detectors.

Our circuit consists of a quantum-well (QW) LED emitting into a waveguide with an SNSPD on the opposite end [see Fig. 1(a)–1(c)]. The device wafer is grown using molecular beam epitaxy. First, a $2\ \mu\text{m}$ layer of highly doped $n\text{-Al}_{0.7}\text{Ga}_{0.3}\text{As}$ is grown on an *n*-type GaAs substrate, followed by 400 nm of intrinsic GaAs with an 11 nm

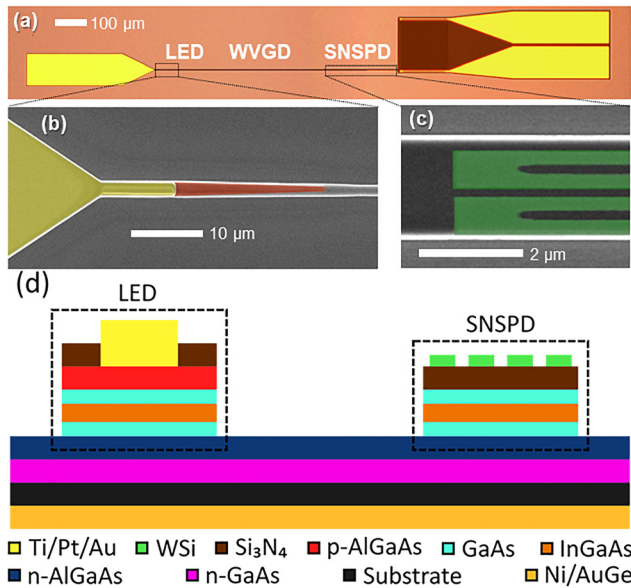


FIG. 1. (a) Microscope image of the integrated source-detector photonic circuit with the light-emitting diode (LED) and the superconducting nanowire single photon detector (SNSPD). (b) and (c) Colorized SEM images of LED and SNSPD. (d) Illustration of the cross section of device layers.

$\text{In}_{0.16}\text{Ga}_{0.84}\text{As}$ quantum well at its center. The diode is completed with 200 nm of $p\text{-Al}_{0.7}\text{Ga}_{0.3}\text{As}$ followed by 20 nm of $p\text{-GaAs}$ to prevent oxidation. Fabrication begins with evaporating and annealing an Ni/AuGe ohmic contact to the backside of the n -doped substrate. The layer of $p\text{-Al}_{0.7}\text{Ga}_{0.3}\text{As}$ is patterned and etched to form the top contact mesas of the LEDs. A 40 nm layer of silicon nitride is deposited to electrically isolate each device. Holes are etched in the nitride spacer to allow current injection into the LEDs from a Ti/Pt/Au top contact layer that is evaporated after this etch step. A 3 nm layer of WSi and a 2 nm layer of amorphous silicon are deposited on the top contacts and etched to form nanowire detectors on top of the waveguides. The waveguide-integrated nanowire is 240 nm wide and runs down the waveguide and back twice to increase absorption, as shown in Fig. 1(c). Finally, the intrinsic GaAs is etched to form the waveguides as well as mesas for the SNSPD inductor meander and contact pads. All patterning was made using i -line photolithography except for the nanowires, which were defined using electron-beam lithography. The yield of our devices was 91%, limited by defects in the nanowire lithography. A cross-sectional overview of the device layers is shown in Fig. 1(d); contact pads for the SNSPDs are omitted for clarity. LEDs were characterized by first performing direct-current-voltage measurements at cryogenic temperatures, shown in Fig. 2(a). The LED turn-on voltage was found to be 2.1 ± 0.2 V at 800 mK, which is slightly higher than the intrinsic bandgap of 1.52 eV and may arise from increased series resistance at low temperatures. LEDs demonstrated a current of less than 100 pA below turn-on and when reverse-biased; the precision of our measurement instruments prevented accurate resolution of smaller currents.

Spectral measurements of LEDs were made by cooling the devices to 5.1 K (unless otherwise stated, all measurements were performed at 800 mK) in an optically accessible, closed-cycle helium cryostat and applying a range of bias currents. Electroluminescence from devices

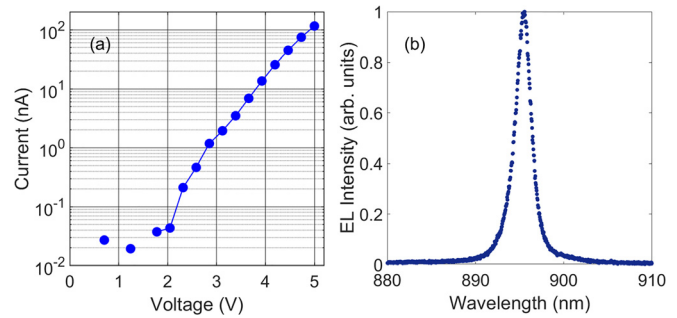


FIG. 2. (a) Light-emitting diode current-voltage measurement at 800 mK. (b) Electroluminescence spectrum at 5.1 K.

designed to scatter light out of the chip was collected by an objective lens and spectrally resolved with a spectrometer and CCD [Fig. 2(b)]. The electroluminescence spectrum is centered at 895 nm with a full-width at half-maximum of 2.1 nm and was not observed to shift spectrally within experimental resolution at different bias currents.

The SNSPDs in our PICs are operated in their superconducting state by providing a constant current slightly lower than their critical current in parallel with a 50 Ω shunt resistor.^{24,25} The critical temperature of WSi is 4.9 K, but the constrained dimensions of the nanowires reduce this to about 3 K.^{20,23} Simulations of the nanowire length, shown in Fig. 3, indicate that a length of 190 nm is sufficient to achieve >99% absorption of the first-order transverse electric (TE) waveguide mode, shown in the inset in Fig. 3. Detector performance was characterized by biasing the SNSPDs at a range of currents and recording the resulting count rate; a plot of these data is shown in Fig. 4. This measurement was performed under two scenarios: first, with the LED coupled to the SNSPD unbiased to measure the dark count rates, and then with the LED operating with various bias currents to measure the SNSPD performance. SNSPD count rates plateau across a 2 μA range of detector bias currents, 70% of the range for which any counts are observed, indicating a saturated internal quantum efficiency.^{12,24} These curves are indicative of high-quality SNSPDs and demonstrate our ability to overcome processing complications arising from patterned and etched substrates. The lengths of the nanowires in our

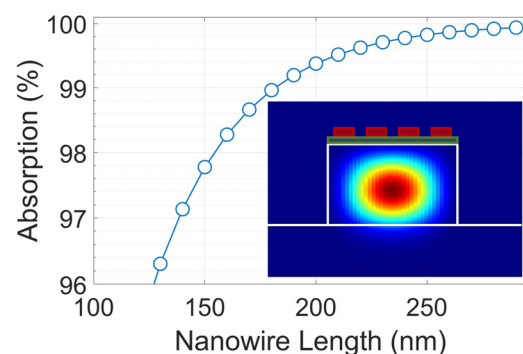


FIG. 3. Simulated absorption of WSi nanowires. Absorption exceeds 99% for nanowires longer than 190 nm. Inset: simulated intensity cross section of the 1st-order TE mode of waveguides. The white box is the GaAs waveguide, the green box is the Si₃N₄ spacer, and the red boxes are the WSi nanowires.

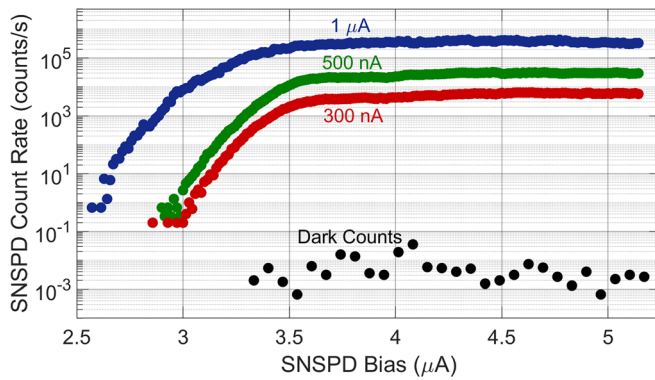


FIG. 4. Measured count rates for SNSPDs at 800 mK with and without LED illumination. The LED was biased at 300 nA, 500 nA, and 1 μ A.

devices were 300 nm and longer, ensuring an absorption probability of $>99.95\%$ (see Fig. 3). Similar WSi SNSPDs have demonstrated internal quantum efficiencies of at least 93%;²¹ we therefore estimate the combined detection efficiency of our detectors to be at least 90%. The reset time of our detectors was 40 ± 5 ns; ignoring the relatively fast dynamics of the LED, this implies a device speed of about 25 MHz. Additionally, the wide plateau allows detectors to operate away from their critical current of 5 ± 0.8 μ A, above which the SNSPDs operate in the normal conducting state, ensuring maximization of the detection efficiency while minimizing dark count rates.²¹ Dark counts measured in the plateau region of bias currents are 7 ± 6 counts/1000 s. Similar PICs using niobium nitride SNSPDs and optically pumped sources exhibit dark count rates near 10 counts/s and suffer from unwanted detection of scattered pump light, leading to background count rates of 10^3 counts/s.¹⁷ While the light sources in our devices are QWs and are therefore brighter than QDs at high injection, the integrated nature of the LEDs greatly reduces the scattered background light. Furthermore, the WSi SNSPDs exhibit low dark count rates that do not change significantly with the bias current. These features of our platform will enable higher signal-to-background ratios with individual quantum emitter sources compared to designs using off-chip excitation and will eliminate the need for careful shielding of the detectors and temporal filtering of scattered light.^{17,18}

Reliable operation of these circuits depends on coupling a sufficient fraction of light generated by LED sources into the waveguide while minimizing the amount of light scattered to other SNSPDs. To ensure that our platform meets these requirements, the cross talk between neighboring PICs was measured by driving one LED and detecting counts from its waveguide-coupled SNSPD as well as counts from the SNSPD on the adjacent waveguide, which is 265 μ m away. A schematic view of this measurement is shown in Fig. 5(a). Data from the cross talk measurement is shown in Fig. 5(b), demonstrating more than 30 dB suppression of count rates on adjacent channels. This ensures light is indeed waveguide coupled and spurious counts from scattered photons are the dominant contribution to the detector noise floor.

The goal of this work was a proof-of-principle demonstration of a fully integrated, source-detector PIC on a III-V platform and system efficiency was not prioritized. The fully integrated nature of our PICs prevents direct measurement of the efficiencies of the individual components, however, we estimate the primary sources of loss to be as follows:

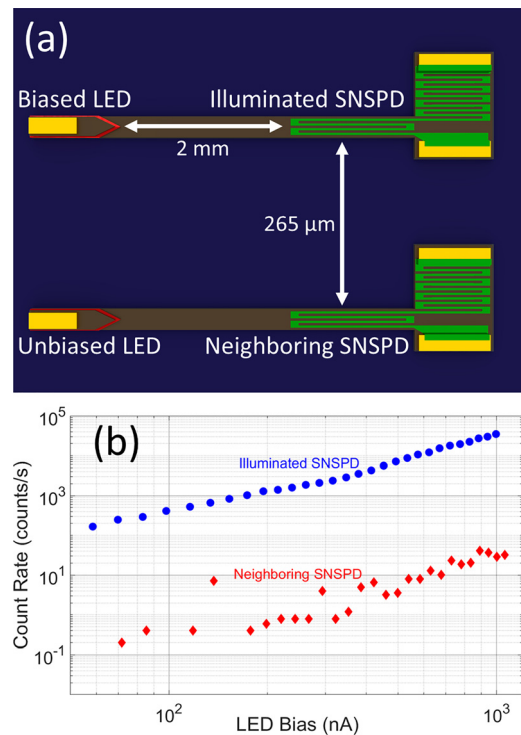


FIG. 5. (a) Schematic view of adjacent devices for cross talk measurement (not to scale). (b) Optical cross talk count rates at 800 mK. The circles represent counts on SNSPD connected to the biased LED. The diamonds represent counts on the neighboring SNSPD.

- (1) The coupling efficiency between the active waveguide region of the LED and the waveguides was estimated using a three-dimensional finite-difference time-domain simulation. The calculated beta factor of the LEDs was about 9×10^{-5} ; the simulation revealed most of the lost light is scattered downward into the substrate, some of which is likely scattered to other SNSPDs and cause the optical cross talk seen in Fig. 5(b). The high sensitivity of the SNSPDs allowed us to sacrifice the coupling efficiency for ease of fabrication, but a PIC platform with single-photon sources necessarily requires a high coupling efficiency to waveguides. Light confinement in the growth direction can be improved by suspending the waveguide, which greatly increases the index contrast.³ Changes to the device geometry to relocate the contact pads and add an etched distributed Bragg reflector behind the current-injection region can more effectively guide light into the waveguide.¹⁴ Another distributed Bragg reflector could be added to the waveguide to form a cavity, making use of the Purcell effect to enhance the emission rate into the waveguide mode.
- (2) Absorption loss within the waveguide is significantly higher in our GaAs waveguides than in silicon.¹⁴ Although the 895 nm light in our PICs is below the bandgap energy of the GaAs waveguides, the InGaAs QW causes absorption and overlaps with the centers of the optical modes. The loss is difficult to estimate with any accuracy at a low temperature because we anticipate a significant, but unknown, Stokes shift of the quantum well exciton emission energy.²⁵ This red-shift of the exciton energy from the peak of the absorption will result in substantially less loss from absorption in the passive regions of the waveguide. This absorption loss could be further mitigated by using intermixing,²⁶ shifting the unpumped

QW band edge from the generated signal photons. Using die- or wafer-bonding enables heterogeneous integration of III-V materials for efficient light generation with silicon-based materials for low-loss routing.^{27,28} The absence of the QW and low absorption of silicon nitride would greatly reduce absorption loss within the waveguide, and the higher index contrast between Si₃N₄ and SiO₂ compared to GaAs/AlGaAs would improve confinement on the bottom interface of the waveguides. While such hybrid platforms reduce absorption loss, they introduce additional loss from interplanar waveguide coupling, which can be made as low as 0.05 dB per coupler.²⁹

- (3) The electro-optical efficiency of the LEDs was not measured in this work, however the increase in the turn-on voltage at low temperatures may indicate freeze out of free carriers. Improvements to the dopant density and material quality can address this issue and would require only a change to the wafer growth. Optimization of the metal-semiconductor contacts would also improve this efficiency by reducing the contact resistance.

Previous examples of III-V platforms for QPICs have used optically pumped quantum dots (QDs) in GaAs as single-photon emitters.^{3,27,30,31} Though our current platform uses an InGaAs QW as the source, changing the epitaxial layer to QDs is straightforward and will be the focus of future studies. Waveguide absorption is also improved by using QDs, as the material absorption of GaAs and resonant absorption by the active layer is less than that of the QW. By choosing the correct density and size of QDs, it may be possible to design an on-chip, electrically injected, waveguide-coupled ensemble of single-photon emitters. It should be noted that to date, the highest-purity single photon emission from QDs has been achieved from resonant optical pumping. The timing jitter resulting from the carrier relaxation induced by non-resonant pumping deteriorates the indistinguishability of single photons. While resonant electrical pumping may be possible using tunneling,³² jitter is still present in the form of the tunneling rate, and further work is necessary before QDs can be used as fully integrated, electrically driven, single-photon emitters. HBT circuits²⁻⁴ and Mach-Zehnder interferometers with phase-modulators³³ could be fabricated on such a platform to measure the single-photon purity and indistinguishability of QD LEDs all on-chip. Photonic crystals have been used to filter single-dot emission from an ensemble on-chip,³ potentially enabling all on-chip measurements of single-dot emission; ring resonators of comparable Q-factor could alternatively be used as well. Photon-number resolving SNSPDs have been integrated with III-V waveguides, providing a path toward complexity scaling of detection circuits while maintaining a small footprint.¹⁹ WSi SNSPDs are well-suited for a III-V platform, as the amorphous material is more tolerant of surface roughness and robust against processing than crystalline NbN.

In summary, we have developed and tested a III-V integrated photonics platform consisting of an all on-chip, all-electrical, source-detector PIC utilizing high-efficiency, WSi SNSPDs with dark count rates below 10⁻³ counts/s and greater than 30 dB optical isolation between adjacent channels. These PICs are scalable and can easily be adapted to include optical structures such as modulators, filters, and beam splitters to enable a breadth of integrated photonics experiments relevant for many applications in science and technology.

REFERENCES

- ¹N. Prtljaga, C. Benthams, J. O'Hara, B. Royall, E. Clarke, L. R. Wilson, M. S. Skolnick, and A. M. Fox, *Appl. Phys. Lett.* **108**, 251101 (2016).
- ²S. Khasminskaya, F. Pyatkov, K. Słowik, S. Ferrari, O. Kahl, V. Kovalyuk, P. Rath, A. Vetter, F. Hennrich, M. M. Kappes *et al.*, *Nat. Photonics* **10**, 727 (2016).

- ³G. E. Digeronimo, M. Petruzzella, S. Birindelli, R. Gaudio, S. F. Poor, F. W. M. van Otten, and A. Fiore, *Photonics* **3**, 55 (2016).
- ⁴M. Schwartz, E. Schmidt, U. Rengstl, F. Hornung, S. Hepp, S. L. Portalupi, K. Ilin, M. Jetter, M. Siegel, and P. Michler, *Nano Lett.* **18**, 6892 (2018).
- ⁵D. J. P. Ellis, A. J. Bennett, C. Dangel, J. P. Lee, J. P. Griffiths, T. A. Mitchell, T. K. Paraiso, P. Spencer, D. A. Ritchie, and A. J. Shields, *Appl. Phys. Lett.* **112**, 211104 (2018).
- ⁶J. W. Silverstone, R. Santagati, D. Bonneau, M. J. Strain, M. Sorel, J. L. O'Brien, and M. G. Thompson, *Nat. Commun.* **6**, 7948 (2015).
- ⁷X. Qiang, X. Zhou, J. Wang, C. M. Wilkes, T. Loke, S. O'Gara, L. Kling, G. D. Marshall, R. Santagati, T. C. Ralph *et al.*, *Nat. Photonics* **12**, 534 (2018).
- ⁸S. Deshpande, T. Frost, A. Hazari, and P. Bhattacharya, *Appl. Phys. Lett.* **105**, 141109 (2014).
- ⁹A. Schlehahn, A. Thoma, P. Munnely, M. Kamp, S. Höfling, T. Heindel, C. Schneider, and S. Reitzenstein, *APL Photonics* **1**, 011301 (2016).
- ¹⁰I. Aharonovich, D. Englund, and M. Toth, *Nat. Photonics* **10**, 631 (2016).
- ¹¹J. P. Sprengers, A. Gaggero, D. Sahin, S. Jahanmirinejad, G. Frucci, F. Mattioli, R. Leoni, J. Beetz, M. Lermer, M. Kamp *et al.*, *Appl. Phys. Lett.* **99**, 181110 (2011).
- ¹²J. M. Shainline, S. M. Buckley, N. Nader, C. M. Gentry, K. C. Cossel, J. W. Cleary, M. Popović, N. R. Newbury, S. W. Nam, and R. P. Mirin, *Opt. Express* **25**, 10322 (2017).
- ¹³J. M. Shainline, S. M. Buckley, R. P. Mirin, and S. W. Nam, *Phys. Rev. Appl.* **7**, 034013 (2017).
- ¹⁴S. M. Buckley, J. Chiles, A. N. McCaughan, G. Moody, K. L. Silverman, M. J. Stevens, R. P. Mirin, S. W. Nam, and J. M. Shainline, *Appl. Phys. Lett.* **111**, 141101 (2017).
- ¹⁵J. Bao, M. Tabbal, T. Kim, S. Charnvanichborikarn, J. S. Williams, M. J. Aziz, and F. Capasso, *Opt. Express* **15**, 6727 (2007).
- ¹⁶F. Flassig, M. Kaniber, G. Reithmaier, K. Müller, A. Andrejew, R. O. Gross, J. Vučković, and J. J. Finley, *Proc. SPIE* **9373**, 937305 (2015).
- ¹⁷G. Reithmaier, M. Kaniber, F. Flassig, S. Lichtmanecker, K. Müller, A. Andrejew, J. Vučković, R. Gross, and J. J. Finley, *Nano Lett.* **15**, 5208 (2015).
- ¹⁸G. Reithmaier, S. Lichtmanecker, T. Reichert, P. Hasch, K. Müller, M. Bichler, R. Gross, and J. J. Finley, *Sci. Rep.* **3**, 1901 (2013).
- ¹⁹D. Sahin, A. Gaggero, Z. Zhou, S. Jahanmirinejad, F. Mattioli, R. Leoni, J. Beetz, M. Lermer, M. Kamp, S. Höfling *et al.*, *Appl. Phys. Lett.* **103**, 111116 (2013).
- ²⁰C. M. Natarajan, M. G. Tanner, and R. H. Hadfield, *Supercond. Sci. Technol.* **25**, 063001 (2012).
- ²¹F. Marsili, V. B. Verma, J. A. Stern, S. Harrington, A. E. Lita, T. Gerrits, I. Vayshenker, B. Baek, M. D. Shaw, R. P. Mirin *et al.*, *Nat. Photonics* **7**, 210 (2013).
- ²²A. D. Beyer, M. D. Shaw, F. Marsili, M. S. Allman, A. E. Lita, V. B. Verma, G. V. Resta, J. A. Stern, R. P. Mirin, S. W. Nam *et al.*, *IEEE Trans. Appl. Supercond.* **25**, 2200805 (2015).
- ²³X. Zhang, A. Engel, Q. Wang, A. Schilling, A. Semenov, M. Sidorova, H.-W. Hübers, I. Charaev, K. Ilin, and M. Siegel, *Phys. Rev. B* **94**, 174509–174501 (2016).
- ²⁴B. Baek, A. Lita, V. Verma, and S. W. Nam, *Appl. Phys. Lett.* **98**, 251105 (2011).
- ²⁵G. Bastard, C. Delalande, M. H. Meynadier, P. M. Frijlink, and M. Voos, *Phys. Rev. B* **29**, 7042 (1984).
- ²⁶E. J. Skogen, J. W. Raring, G. B. Morrison, C. S. Wang, V. Lal, M. L. Mašanović, and L. A. Coldren, *IEEE J. Sel. Top. Quantum Electron.* **11**, 343 (2005).
- ²⁷M. Davanco, J. Liu, L. Sapienza, C. Zhang, J. V. D. Cardoso, V. Verma, R. Mirin, S. W. Nam, L. Liu, and K. Srinivasan, *Nat. Commun.* **8**, 889 (2017).
- ²⁸T. Komljenovic, M. Davenport, J. Hulme, A. Y. Liu, C. T. Santis, A. Spott, S. Srinivasan, E. J. Stanton, C. Zhang, and J. E. Bowers, *J. Lightwave Tech.* **34**, 20 (2016).
- ²⁹J. Chiles, S. Buckley, N. Nader, S. W. Nam, R. P. Mirin, and J. M. Shainline, *APL Photonics* **2**, 116101 (2017).
- ³⁰I. E. Zadeh, A. W. Elshaari, K. D. Jöns, A. Foghini, D. Dalacu, P. J. Poole, M. E. Reimer, and V. Zwiller, *Nano Lett.* **16**, 2289 (2016).
- ³¹J. Kim, S. Aghaeimeibodi, C. J. K. Richardson, R. P. Leavitt, D. Englund, and E. Waks, *Nano Lett.* **17**, 7394 (2017).
- ³²O. Benson, C. Santori, M. Pelton, and Y. Yamamoto, *Phys. Rev. Lett.* **84**, 2513 (2000).
- ³³J. Wang, A. Santamato, P. Jiang, D. Monneau, E. Engin, J. W. Silverstone, M. Lermer, J. Beetz, M. Kamp, S. Höfling *et al.*, *Opt. Commun.* **327**, 49 (2014).